Vol. 87: 167–183, 2021
https://doi.org/10.3354/ame01977

AQUATIC MICROBIAL ECOLOGY
Aquat Microb Ecol

Published online October 21

Effects of nutrient enrichments on oligotrophic phytoplankton communities: a mesocosm experiment near Hawai'i, USA

Daniela Böttjer-Wilson[1,#], Angelicque E. White[2,3,#,*], Karin M. Björkman[2,3], Matthew J. Church[4], Steve Poulos[2,3], Eric Shimabukuro[2,3], Yoshimi M. Rii[5], Andrea Ludwig[6], Klaus von Bröckel[6], Ulf Riebesell[6], Ricardo M. Letelier[7], David M. Karl[2,3]

[1]Center for Teaching Excellence, University of Hawai'i at Mānoa, Honolulu, Hawai'i 96822, USA
[2]Department of Oceanography, School of Ocean and Earth Science and Technology, University of Hawai'i at Mānoa, Honolulu, Hawai'i 96822, USA
[3]Daniel K. Inouye Center for Microbial Oceanography: Research and Education, University of Hawai'i at Mānoa, Honolulu, Hawai'i 96822, USA
[4]Flathead Lake Biological Station, University of Montana, Polson, Montana 59860, USA
[5]Hawai'i Institute of Marine Biology, University of Hawai'i at Mānoa, Kaneohe, Hawai'i 96744, USA
[6]GEOMAR Helmholtz Centre for Ocean Research Kiel, 24148 Kiel, Germany
[7]College of Earth, Ocean and Atmospheric Sciences, Oregon State University, Corvallis, Oregon 97331, USA

ABSTRACT: A large-volume mesocosm-based nutrient perturbation experiment was conducted off the island of Hawai'i, USA, to investigate the response of surface ocean phytoplankton communities to the addition of macronutrients, trace metals, and vitamins and to assess the feasibility of using mesocosms in the open ocean. Three free-drifting mesocosms (~60 m^3) were deployed: one mesocosm served as a control (no nutrient amendments); a second (termed +P) was amended with nitrate (N), silicate (Si), phosphate (P), and a trace metal + vitamin mixture; and a third (termed –P) was amended with N, Si, and a trace metal + vitamin mixture but no P. These mesocosms were unreplicated due to logistical constraints and hence differences between treatments are qualitative. After 6 d, the largest response of the phytoplankton community was observed in the +P mesocosm, where chlorophyll *a* and ^{14}C-based primary production were 2–3× greater than in the –P mesocosm and 4–6× greater than in the control. Comparison between mesocosm and 'microcosm' incubations (20 l) revealed differences in the magnitude and timing of production and marked differences in community structure with a reduced response of diatoms in microcosm treatments. Notably, we also observed pronounced declines in *Prochlorococcus* populations in all treatments, although these were greater in microcosms (up to 99%). Overall, this study confirmed the feasibility of deploying free-drifting mesocosms in the open ocean as a potentially powerful tool to investigate ecological impacts of nutrient perturbations and constitutes a valuable first step towards scaling plankton manipulation experiments.

KEY WORDS: Phytoplankton · Nutrient dynamics · Mesocosm · North Pacific Subtropical Gyre

1. INTRODUCTION

The availability of dissolved inorganic nutrients is a key determinant of the abundance and activity of photosynthetic microorganisms in the global ocean, and consequently sets the magnitude of particulate and dissolved organic matter production in the euphotic zone (Redfield 1958). Downward transport of living or detrital organic material (export) out of the euphotic zone acts to fuel microbially mediated re-

[#]These authors contributed equally to this work
[*]Corresponding author: aewhite@hawaii.edu

Publisher: Inter-Research · www.int-res.com

mineralization processes that ultimately return nutrients from particulate to dissolved forms and can lead to the net sequestration of carbon (C) from the atmosphere (Moore et al. 2013). For this reason, nutrient perturbations aimed at manipulating ocean production and potentially enhancing C export to the interior waters are of enormous public and scientific interest (Boyd 2008, Taucher et al. 2018). For instance, artificial enrichments of the surface ocean with deep, nutrient-rich waters have been proposed as a mechanism to stimulate phytoplankton blooms and support the drawdown of atmospheric carbon dioxide (CO_2) (Lovelock & Rapley 2007, Vaughan & Lenton 2011). However, these deep waters are also enriched in CO_2 that would be released into the atmosphere when brought to the surface and counter the intended C sequestration (Takahashi et al. 1997, Karl & Letelier 2008). This is why, for example, upwelling zones are net sources of CO_2 to the atmosphere whereas more persistently stratified regions, including the subtropical gyres, tend to be net CO_2 sinks. The magnitude, rate, and stoichiometry (elements:metals:vitamins) of nutrient supply as well as the initial plankton community composition (from autotrophs to grazers) and biological demand are all important determinants of the ultimate successional patterns (e.g. Estrada et al. 2003) and the biomass yield and potential export in response to natural and artificial nutrient additions (Smith & Mackenzie 1991, Sunda 2012, Moore et al. 2013). For example, Karl & Letelier (2008) argued that the chemical composition of the source water, and specifically the nitrogen:phosphorus (N:P) ratio, utilized in nutrient perturbation experiments can be critical to achieving net export and in avoiding unintended ecological consequences such as the formation of toxin-producing microorganisms or shifts in the planktonic community structure that might alter trophic interactions in unforeseen ways.

To date, the majority of experimental manipulations investigating the response of planktonic assemblages to inorganic nutrient additions have been conducted in bottles ranging from 1 to 20 l (here termed 'microcosms'). These relatively small-volume incubations have the advantage that they can be highly controlled, and precisely replicated (Boyd et al. 2018). However, such microcosms also often result in significant perturbations of trophodynamic interactions (e.g. reducing predation or eliminating 'rare' organisms), or deviations from *in situ* light, temperature, and mixing regimes (Hecky & Kilham 1988). Larger-scale enclosures such as mesocosms have the benefit that they allow study of a multi-trophic level ecosystem in the same water mass over an extended period of time under *in situ* settings (Gamble & Davies 1982), enabling more robust ecological inferences over longer time-scales (Riebesell et al. 2010, Boyd et al. 2018). By enclosing a larger volume of water (up to ~1000 m^3), mesocosm experiments often permit greater sampling frequency and/or sampling of a larger number of properties. While large-volume experiments may be limited in replication/factorial design, for example in the case of artificial iron-addition experiments (Hale & Rivkin 2007), they are still considered a powerful approach to examine ecosystem-level responses to ecological perturbations (Riebesell et al. 2010, Boyd et al. 2018).

In December 2011, a large-volume nutrient perturbation experiment (termed Biogeochemistry And Genomes-1, BAG-1) was conducted during a research expedition in waters off Hawai'i, USA, using 3 free-drifting mesocosms (60 m^3). In addition, we conducted smaller volume (20 l) microcosm nutrient-amendment experiments for comparison. These experiments were intended to examine phytoplankton responses to the addition of nutrient mixtures including those with P (+P) and without P (–P) and how these responses scale from microcosms to mesocosms. This region is typical of the broader North Pacific Subtropical Gyre (NPSG) in the sense that (1) surface chlorophyll concentrations are low (at or <0.1 µg l^{-1}) and there is a predominance of small cell-sized phytoplankton, (2) the mixed layer is shallow (generally <45 m), (3) nutrient concentrations are persistently low in the upper euphotic zone and often at or below the detection limits of standard analytical methods (nmol l^{-1}), and (4) there is a chlorophyll *a* (chl *a*) maximum at ~125 m at the intersection of the depth of the euphotic zone and the nitracline (Letelier et al. 2004, Rii et al. 2008). This nutrient-poor and logistically accessible region of the NPSG provided a unique opportunity to test the engineering and feasibility of utilizing these mesocosms in potentially exposed open-ocean conditions for the first time. Prior tests of these mesocosms have all been conducted in enclosed bays or fjords with limited currents and wind stress (Riebesell et al. 2013) and were oriented to understanding the response of plankton to CO_2 perturbations (Endres et al. 2014, Crawfurd et al. 2017), but none have examined plankton growth in the oligotrophic open ocean.

2. MATERIALS AND METHODS

2.1. Description of mesocosms

The 3 mobile, sea-going mesocosm units utilized were those designed and developed as part of the Kiel

Off-Shore Mesocosms for Future Ocean Simulations (KOSMOS) at GEOMAR in Kiel, Germany (Riebesell et al. 2013). Briefly, each free-drifting mesocosm structure, 8.5 m high and 2.8 m in diameter, consisted of a flotation frame made out of reinforced fiberglass tubes and stainless steel and outfitted with a ~3 mm thick × 20 m long flexible bag made from thermoplastic polyurethane (Fig. 1A). During deployment, the bag was folded and hanging inside the flotation frame, attached by ropes and secured by tension belts to prevent swinging. Once the mesocosm unit was deployed, the bag was unfolded by weights pulling down its lower end to depth, thereby enclosing a water column of approximately 60 m^3 in volume. Divers then closed the bag at the bottom by attaching a funnel (~2 m in length) that served for collection of sinking material. A positively buoyant rope connected the mesocosms. Since this cruise represented the first attempt to deploy the mesocosm array in a free-drifting mode, a drogue anchor was attached to the array with the goal of maintaining separation between the 3 mesocosms and preventing entanglement. The drogue anchor (Fig. 1B) consisted of a hard surface buoy capable of offsetting ~150–250 kg of weight, an underwater drifter installed well below the surface currents (~150 m depth) that served as a sail, and a small weight (about 40 kg) at the bottom of the underwater drifter. The surface expression of the drogue anchor included lights (for visibility of the mesocosm array at night), radar reflectors, and a satellite positional tracking (ARGOS) unit.

2.2. Deployment of mesocosm array

The BAG-1 expedition departed Honolulu, HI, on 3 December 2011 aboard the RV *Ka'imikai-O-Kanaloa*, transiting southeast to the leeward coast of the island of Hawai'i. Upon arrival, the mesocosms were deployed (Fig. 1C) ~15 km off the coast of Kailua-Kona (19.64° N, 156.19° W) on the eastern edge of an anticyclonic eddy with low wind speeds of ~13 km h^{-1} (Fig. 2). The location for the deployment was chosen to help constrain the drift track of the free-drifting mesocosm array and keep it in relatively calm waters with swell and wind waves less than 2

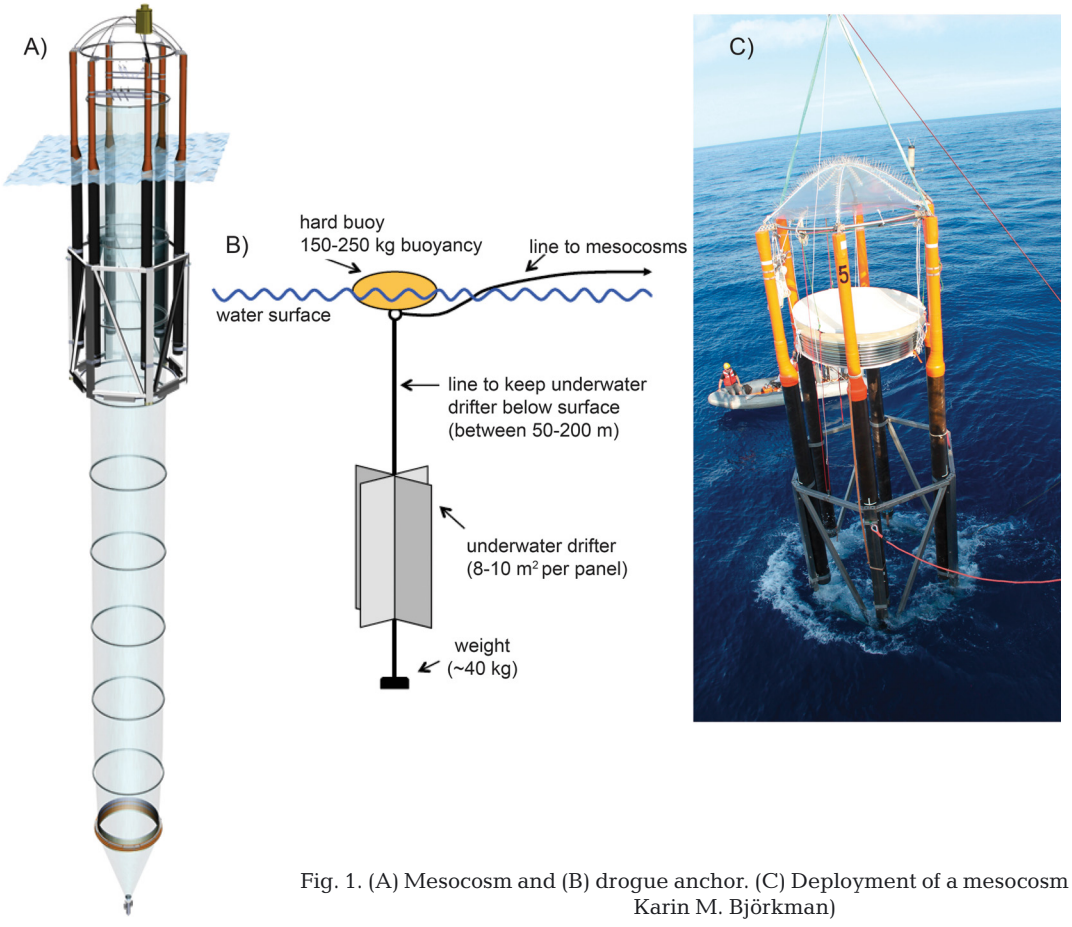

Fig. 1. (A) Mesocosm and (B) drogue anchor. (C) Deployment of a mesocosm (photo by Karin M. Björkman)

m. Mesocosm deployments were followed by the deployment of the drogue anchor. Shortly after, the mesocosm bags were unfolded at the top of the mesocosm frame and slowly sank through the water column. For free exchange with the surrounding water masses, the mesocosms were left open for a period of ~24 h before they were closed. The closure of the mesocosm bags marked the beginning date of the experimental period, 5 December 2011.

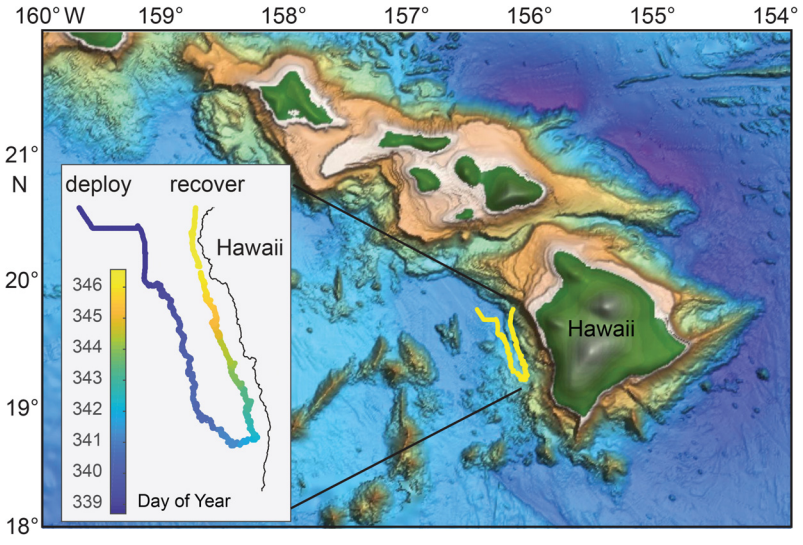

Fig. 2. Location of deployment and recovery (colored by day of year over the deployment period in the inset) relative to bathymetry along with the drift pattern seen as a yellow line and expanded in the inset to show deployment duration of the mesocosm array off Kona, Hawai'i, USA, during the BAG-1 campaign in December 2011. Bathymetry and topography (scales not shown) were obtained from the combination of the multibeam synthesis along with USGS digital elevation models and the Smith and Sandwell Measured and Estimated Seafloor Topography (www.soest.hawaii.edu/HMRG/multibeam/bathymetry.php)

Table 1. Final concentrations of macronutrients, trace metals, and vitamins added to the nutrient-amended micro- and mesocosms (–P and +P) that simulated the addition of 15% deep-sea water from Stn ALOHA (1000 m)

Added chemical compound	Final concentration
Sodium nitrate ($NaNO_3$)	6 µmol l^{-1}
Monopotassium phosphate (KH_2PO_4)	0.5 µmol l^{-1} [a]
Sodium fluorosilicate (Na_2SiF_6)	14 µmol l^{-1}
Ferric chloride hexahydrate ($FeCl_3 * 6H_2O$)	0.1 nmol l^{-1}
Zinc sulfate heptahydrate ($ZnSO_4 * 7H_2O$)	1 nmol l^{-1}
Selenous acid (H_2SeO_3)	0.3 nmol l^{-1}
Nickel (II) sulfate hexahydrate ($NiSO_4 * 6H_2O$)	1.5 nmol l^{-1}
Cobalt (III) chloride hexahydrate ($CoCl_2 * 6H_2O$)	9 pmol l^{-1}
Thiamin (Vitamin B_1)	2.3 pmol l^{-1}
Biotin (Vitamin B_7)	3.5 pmol l^{-1}
Cobalamin (Vitamin B_{12})	0.5 pmol l^{-1}

[a]Added to the +P mesocosm only

2.3. Experimental design and sampling strategy

Nutrient amendments were intended to enhance biomass and growth and to allow an examination of change in phytoplankton community structure in mesocosms and the more commonly used microcosms; a P-free treatment was also included to evaluate how P influences N drawdown or changes in community structure (see Karl et al. 2001, Letelier et al. 2019). Macronutrients and trace elements were added to both microcosms and mesocosms (Table 1). The artificial nutrient mixtures were prepared in 0.2 µm filtered surface seawater collected prior to the cruise (from ~300 m at Stn ALOHA, the field-site of the Hawai'i Ocean Time-series program; 22.75° N, 158° W). Stock solutions of the various macronutrients, trace metals, and vitamins were prepared in deionized water (18.2 MΩ cm^{-1}).

The limited number of mesocosm units available during the present study (n = 3) did not allow for replication of the experimental treatments. One mesocosm served as a control containing unamended seawater, a second mesocosm was enriched with a nutrient mixture that included nitrate (NO_3^-, abbreviated as N), silicate (Si), trace metals, and vitamins, but lacking in phosphate (PO_4^{3-}, the –P treatment); and a third mesocosm was amended with the same nutrient mixture but inclusive of P (the +P treatment). The nutrient mixtures were injected into 2 of the 3 mesocosms utilizing a membrane pump together with a dispensing device termed a 'spider' (for details, see Fig. 7 in Riebesell et al. 2013). The 'spider' allows for even distribution of added nutrients vertically throughout the entire mesocosm by moving the device slowly up and down during the injection process. Daily sampling of the mesocosms was conducted from aboard a small boat starting prior to dawn (~06:30 h) and finishing after approximately 4 h (~11:00). Vertical profiles of temperature, salinity, pH, and fluorescence were obtained from each mesocosm as well as from the surrounding Pacific Ocean using a hand-

held, multi-parameter probe (CTD60M, Sun and Sea Technologies). A total volume of approximately 50 l of seawater was subsampled from each mesocosm for subsequent discrete biogeochemical analyses (see Sections 2.5–2.8) using a depth-integrating water sampler (Hydro-Bios; 5 l volume), which collects water continuously while being lowered from the surface to the bottom of the bag (~25 m). Seawater properties needed to assess potential contamination (e.g. inorganic nutrients) were directly sampled from the integrating sampler, whereas seawater for the remaining measurements was transferred into 10 l polyethylene containers and subdivided for further sample processing back on the research vessel. Prior to each instrumental deployment, sampling gear was immersed into the ocean surrounding the mesocosms to avoid cross-contamination between nutrient-enriched and control mesocosms. The full suite of biogeochemical measurements was also conducted in the near-surface of surrounding Pacific waters.

2.4. Description of microcosms

In addition to the large-scale *in situ* mesocosm experiment, a deck-board microcosm experiment was set up that allowed us to evaluate potential differences attributable to incubation vessel size. For this, approximately 350 l of surface seawater were collected from 15 m depth using a conductivity-temperature-depth (CTD) rosette sampler (19.4° N, 156.1° W, within 5 km of the mesocosms) and subsampled into 12 acid-washed 20 l polycarbonate carboys. After filling, carboys were enriched with the same nutrient mixtures as the mesocosms (–P and +P treatments in addition to unamended controls) and placed in shaded (~50 % surface irradiance), surface seawater-cooled incubators on deck of the research vessel. At each designated time point (T_2, T_4, T_6, T_7 with intervals in units of days), a single carboy per treatment was sacrificed and sub-sampled for selected biogeochemical measurements including dissolved and particulate nutrients, chl *a*, ^{14}C-based primary production (PP), and diagnostic pigments. Here, we compare only the first 6 d of data to match the duration of the mesocosms.

2.5. Dissolved inorganic nutrients and particulates

Samples for analyses of dissolved inorganic nutrient concentrations (nitrate plus nitrite = $[NO_3^- + NO_2^-]$, $[PO_4^{3-}]$, and silicate = $[Si(OH)_4]$) were sampled into clean, acid-washed 500 ml polyethylene bottles, capped, and immediately frozen upright at –20°C. At the shore-based laboratory, these samples were thawed and run on a Bran and Luebbe Autoanalyzer III to determine $[NO_3^- + NO_2^-]$, $[PO_4^{3-}]$, and $[Si(OH)_4]$. Note that we refer to the chemical ions rather than N or P when referring specifically to measured nutrient concentrations.

Seawater samples for the determination of particulate carbon (PC) and nitrogen (PN) were pre-screened (202 µm Nitex® mesh) and subsequently positive pressure filtered (30–45 kPa nitrogen gas) through in-line combusted 25 mm GF/F filters. Whole (not pre-screened so as not to exclude large diatoms) seawater samples for particulate biogenic silica (PSi) were pressure filtered onto 0.8 µm pore size, 47 mm diameter polycarbonate membrane filters. All samples were stored frozen (–20°C) until analyzed. In the laboratory, filters for PC and PN were dried for 24 h at 60°C, pelleted, and measured via the high-temperature combustion method described by Grabowski et al. (2019). PSi concentrations were measured colorimetrically following the protocol of DeMaster (1981).

2.6. Size-fractionated chl *a* and ^{14}C-based primary productivity (PP)

Seawater samples for chl *a* were subsampled into 150 ml amber polyethylene bottles and filtered onto 25 mm diameter GF/F filters. Samples for size-fractionated chl *a* analysis were collected into larger amber polyethylene bottles (1 l), and the entire volume was sequentially filtered by positive pressure through in-line, 25 mm diameter, 10 and 2 µm pore size polycarbonate filters. The <2 µm filtrate was collected, and 150 ml of this filtrate were subsequently vacuum-filtered onto 25 mm diameter, 0.2 µm pore size polycarbonate filters. All filters were transferred into 10 ml glass screw-cap tubes containing 5 ml of cold (–20°C) 100 % acetone. Tubes were wrapped in aluminum foil and stored at –20°C for approximately 7 d to passively extract pigments (Letelier et al. 1996). Back in the shore-based laboratory, chl *a* concentrations were determined fluorometrically via the acid method of Holm-Hansen et al. (1965).

The ^{14}C-radiotracer technique (Steemann Nielsen 1952) was applied to measure the assimilation of inorganic C by phytoplankton as an estimate of the rate of PP, following the procedures described by Letelier et al. (1996). Sample bottles (500 ml bottles filled with no void) were incubated in outdoor, light-shaded (~50 % surface irradiance), seawater-cooled

incubators for the entire photoperiod (~12 h). After dusk, 250 µl of the incubated seawater were removed from each bottle and placed into 20 ml glass scintillation vials containing 500 µl β-phenethylamine (Sigma-Aldrich) for subsequent determination of the total ^{14}C activity in each sample. A 100 ml aliquot was filtered through 25 mm diameter GF/F; we consider this sample to represent total PP. The remaining sample volume (~400 ml) was subsequently filtered through 25 mm diameter, 10 and 2 µm pore size polycarbonate filters (representing the >10 µm and 2–10 µm fraction, respectively). The <2 µm filtrates were retained, and 250 ml of each filtrate were then filtered onto 25 mm diameter, 0.2 µm pore size filters (representing the 0.2–2 µm fraction). All filters were placed into scintillation vials and stored at –20°C. At the shore-based laboratory, filters were acidified by the addition of 1 ml of 2 M hydrochloric acid and allowed to passively vent in a fume hood for 24 h. To determine the ^{14}C activity, scintillation vials received 10 ml of liquid scintillation cocktail (Ultima Gold LLT©, Perkin-Elmer) and were counted in a liquid scintillation counter (Perkin-Elmer 2770XL) after a 30 d period. Dissolved inorganic carbon concentrations were measured for each incubation and were on average 2047 ± 4 (SD) (n = 24) µmol l^{-1}. PP was calculated as per Letelier et al. (1996).

2.7. Photosynthetic pigment determinations

Photosynthetic pigments (chlorophylls and carotenoids) were determined by high-performance liquid chromatography (HPLC). Samples were collected into amber, narrow-mouthed 2 l polyethylene bottles, vacuum-filtered onto 25 mm GF/F filters, and subsequently stored in liquid nitrogen at –80°C until analysis. Samples were processed and analyzed following the method outlined by Bidigare et al. (2005). Filters were extracted in 100% acetone for 24 h at –20°C. Extracts were processed in reverse phase on a Grace C8 column using a Waters separations module and photodiode detector array with Empower chromatography software. Pigment to chl *a* ratios were derived by normalizing pigment concentrations of 19′-hexanoyloxyfucoxanthin, 19′-butanoyloxyfucoxanthin, and fucoxanthin to monovinyl chl *a* concentrations.

2.8. Plankton community structure

Abundance and composition of picoplankton assemblages (generally <2 µm) were determined by flow cytometry. Seawater samples from each mesocosm, microcosm, and the surrounding water column were collected into 2 ml cryovials containing 30 µl of 0.2 µm prefiltered paraformaldehyde (final concentration = 0.24%). Fixed samples were left in the dark at room temperature for approximately 15 min, then flash-frozen in liquid nitrogen and subsequently stored at –80°C until shore-based analysis. In the laboratory, frozen samples were thawed and counted on a Cytopeia Influx Mariner flow cytometer. Forward light scatter (FLS), red fluorescence (692 nm), and orange fluorescence (580 nm) were detected and quantified, and the enumeration and fluorescence data were analyzed using FlowJo software (Tree Star). Abundances of non-pigmented picoplankton (hereafter referred to as heterotrophic bacteria, HBAC) were determined based on SYBR Green (Molecular Probes) stained total cell abundances following the subtraction of unstained *Prochlorococcus* cell counts. Based on FLS and relative fluorescence, cells that contained chl *a* were distinguished into 3 different groups: *Prochlorococcus* (PRO), *Synechococcus* (SYN), and photosynthetic picoeukaryotes (PEUK, which while termed 'pico' by convention also include cells up to ~6 µm [Worden & Not 2008]). SYN was further differentiated by orange fluorescence, whereas PEUK were distinguished from the relatively smaller cyanobacteria (PRO+SYN) by greater FLS and red fluorescence.

Abundances and species composition of microphytoplankton (>20 µm) were determined using light microscopy. From each mesocosm and the surrounding Pacific Ocean, 1 l of seawater was collected daily and gravity-filtered through a 20 µm Nitex® mesh. Particles collected on the mesh were washed off with filtered seawater into an Utermöhl counting chamber and were allowed to settle for at least 2 h before cell enumeration using a Zeiss Axiovert 25 inverse light microscope (Edler & Elbrächter 2010). In most cases, the entire bottom of the settling chamber was scanned for cell counting, and phytoplankton cells were classified to the lowest possible taxonomic level (species or genus). Cell enumeration was restricted to half of the settling chamber in cases where >100 cells of the dominant species were counted at that stage.

3. RESULTS

3.1. Hydrographic conditions

Daily vertical profiles of temperature, salinity, pH, oxygen, and fluorescence were obtained from each mesocosm (~20 m depth) using a handheld CTD with

a 5 Hz sampling rate; data were only used from the downcast. During the time course of the experiment, the average temperatures in the 3 mesocosms ranged between 25.0 and 25.2°C (Tables S1–S3 in the Supplement at www.int-res.com/articles/suppl/a087p167_supp.xlsx). Similarly, salinity and pH levels in the mesocosms were homogeneously distributed with depth, and remained relatively constant throughout the time course of the experiment (Tables S1–S3). The upper 20 m of the surrounding seawater was also well mixed, with little variability in temperature and salinity over the sampling period (Δ of <0.1°C and <0.02, respectively, in the upper 20 m; Table S4).

3.2. Mesocosm drift track

After deployment southwest of the island of Hawai'i, the mesocosm array initially drifted within an anticyclonic eddy at a speed of 0.93 km h^{-1} to the southeast (Fig. 2). However, after approximately 2 d, the drift track obtained from the acoustic Doppler current profiler showed the drifting mesocosm array beginning to leave the eddy and moving at a slower speed (0.6 km h^{-1}) further to the east. At the same time, the wind speed decreased from ~13 to 7.4 km h^{-1}. At the beginning of Day 3, the mesocosm array drifted free of the southeasterly eddy, moving to the north. Following this diversion to the north, the array drifted into even calmer waters, riding a counter current north up along the coast of the island of Hawai'i, approximately 4.8 km offshore. The array eventually drifted towards shallow waters (~100 m depth) and the drogue anchor ran aground; this required termination of the experiment since we determined we could not reposition the array.

Overall, the chosen location for deployment was favorable in terms of the sea state we deemed ideal for this operation (range of wind speed: 20–30 km h^{-1}, wave height: 1–2 m). The mesocosms behaved well in currents with often changing directions and were capable of handling swells of up to 2 m, making sampling possible at all times. Observations made during the campaign suggested that swell or wind waves >3 m set the limit for the current mesocosm configuration. We also tested the utilization of a weighted drogue anchor lowered to 150 m depth alongside the mesocosms with the goal of generating ample and constant force on one side of the drifting array to keep the 3 mesocosms in a straight line. Its application successfully prevented the mesocosms from entangling; however, operating such a drogue in waters close to shore requires careful monitoring of the water depth and timely lifting of the drogue when entering shallow waters. Unfortunately, in the present campaign, the drogue got caught and with the array stuck at one end, the current pulled the mesocosms below the sea surface. When submerged, seawater from the surrounding water entered the mesocosms; as a result, the experiment was terminated.

3.3. Dissolved and particulate nutrient dynamics

The initial concentrations of dissolved inorganic nutrients prior to additions were as follows: ~0.05 µmol l^{-1} [NO_3^- + NO_2^-], ~0.13 µmol l^{-1} [PO_4^{3-}], and ~1.2 µmol l^{-1} [$Si(OH)_4$]. These initial concentrations and the variability of nutrient concentrations in controls did not differ from the surrounding waters (Table S8, 0.05 ± 0.01 µmol l^{-1} [NO_3^- + NO_2^-], 0.13 ± 0.00 µmol l^{-1} [PO_4^{3-}], and ~1.5 ± 0.05 µmol l^{-1} [$Si(OH)_4$]). The addition of NO_3^- and $Si(OH)_4$ to the –P and +P treatments increased those concentrations to ~6.4 µmol l^{-1} [NO_3^- + NO_2^-] and ~12 µmol l^{-1} [$Si(OH)_4$] in the mesocosms and to ~6.0 µmol l^{-1} [NO_3^- + NO_2^-], and ~11 µmol l^{-1} [$Si(OH)_4$] in the microcosms, respectively (Table 2). The addition of PO_4^{3-} (+P treatments) increased concentrations to 0.65 µmol l^{-1} in the +P mesocosm and to ~0.5 µmol l^{-1} in the +P microcosm.

Over the time course of the mesocosm experiment, [NO_3^- + NO_2^-] and [PO_4^{3-}] decreased by 0.47 and 0.02 µmol l^{-1}, respectively, in the –P treatment as compared to a decline of 1.0 µmol l^{-1} [NO_3^- + NO_2^-] and 0.05 µmol l^{-1} [PO_4^{3-}] in the +P mesocosm (Fig. 3). Consumption of these nutrients was partially reflected in increases in PN (accounting for 83 and 65% of the [NO_3^- + NO_2^-] drawdown in –P and +P mesocosms, respectively). The N:P stoichiometry of net nutrient consumption was similar (20.2 and 18.8 mol:mol for –P and +P) between experimental treatments.

Consumption of NO_3^- + NO_2^- in the microcosm experiment (Table 2, Fig. 3) was greater in the –P compared to the +P treatment; [NO_3^- + NO_2^-] decreased by 1.1 µmol l^{-1} as compared to a 0.5 µmol l^{-1} decline for the +P treatment. Conversely, [PO_4^{3-}] decline was greater (0.05 µmol l^{-1}) in the +P treatment as opposed to the –P treatment (0.04 µmol l^{-1}). The N:P molar drawdown ratio was above Redfield in the –P treatment (29.8) and below Redfield in the +P treatment (10.2). The increase in PN accounted for 21% (–P) and 56% (+P) of the net removal of [NO_3^- + NO_2^-] (Table 2). In all nutrient-enriched mesocosms and microcosms, an increase in PSi was observed

Table 2. Summary of dissolved and particulate nutrient inventories in the nutrient-amended micro- and mesocosms at the beginning (T_0) and end (T_F) of the experiment; Δ describes the difference between both time points (6 d duration) and are noted in *italics*. N+N: nitrate plus nitrite; PO_4^{3-}: phosphate; PN: particulate nitrogen; $Si(OH)_4$: silicate; and PSi: particulate biogenic silicate. For mesocosm data, initial particulates were the mean value measured in the surrounding Pacific water (Table S8). For microcosm data, initial particulate data were from the initial CTD sampling at the start of all microcosm incubations from which all samples originated, and time-zero nutrient levels are estimated from nutrient additions (all raw data are provided in Table S8)

	Mesocosm			Microcosm		
	Control	–P	+P	Control	–P	+P
Dissolved (μmol l^{-1})						
T_0 N+N	0.05	6.30	6.49	0.05	6.00	6.00
T_F N+N	0.05	5.84	5.50	0.01	4.86	5.48
Δ N+N	*0.00*	*–0.46*	*–1.01*	*–0.04*	*–1.14*	*–0.52*
T_0 PO_4^{3-}	0.13	0.14	0.65	0.13	0.13	0.50
T_F PO_4^{3-}	0.13	0.11	0.59	0.13	0.09	0.45
Δ PO_4^{3-}	*0.00*	*–0.02*	*–0.05*	*0.00*	*–0.04*	*–0.05*
T_0 $Si(OH)_4$	1.24	11.51	12.38	1.24	10.50	10.28
T_F $Si(OH)_4$	1.17	11.65	12.31	1.08	9.82	10.11
Δ $Si(OH)_4$	*–0.07*	*+0.15*	*–0.07*	*–0.16*	*–0.68*	*–0.39*
Particulate (nmol l^{-1})						
T_0 PN	361	361	361	651	651	651
T_F PN	393	748	1014	527	892	941
Δ PN	*+31*	*+386*	*+652*	*–125*	*+240*	*+289*
T_0 PSi	20	20	20	24	24	24
T_F PSi	29	126	127	13	49	66
Δ PSi	*+9*	*+106*	*+107*	*–11*	*+25*	*+42*

(see Table S10); however, this increase was 2–4× more pronounced in mesocosm treatments as compared to microcosms (Table 2).

3.4. Dynamics of chl *a* concentrations and rates of ^{14}C-based PP

Standing stocks and the ^{14}C-based PP of the various size-classes of autotrophic microorganisms were stimulated by the nutrient, trace metal, and vitamin mixtures added to the –P and +P micro- and mesocosms. Typical for the study site, most of the chl *a* and PP throughout both experiments was attributed to microorganisms <2 μm in size, presumably *Prochlorococcus* and *Synechococcus*, as shown by size-fractionated estimates (Figs. 4 & 5, Tables S5 & S7). Concentrations of chl *a* and rates of PP were greatest in the +P mesocosm. Their maxima (~0.4 μg chl *a* l^{-1} d^{-1} and 29 mg C m^{-3} d^{-1}) occurred during the middle of the experiment (Day 4) and were ~2–3× higher than in the –P mesocosm and 4–6× higher compared to the control mesocosm (Figs. 4 & 5). Subsequently, chl *a* and PP generally leveled off and/or declined, except for the >10 μm size fraction in the +P mesocosms, which showed a steady increase in PP beginning on Day 2 of the experiment (Figs. 4 & 5). This roughly 8× increase over the time course of the experiment suggests growth of larger eukaryotic microorganisms in response to added N, P, vitamins, and trace metals. Given the ~100 nmol l^{-1} increase in PSi in mesocosm treatments, we suspect increases in chl *a* and PP in the larger filter size fraction reflect net growth of diatoms in the nutrient-amended mesocosms.

Calculating cumulative production (the sum of 1–6 d rates), the total +P mesocosm had ~5× the production (116 mg C m^{-3}) of the controls (26 mg C m^{-3} in the control mesocosm and 21 mg C m^{-3} in the Pacific) and ~2× the production of the –P mesocosm (59 mg C m^{-3}), even though the relative contributions of the various size fractions were consistent between treatments (<2 μm = 48 ± 9% [SD], 2–10 μm = 32 ± 7%, and >10 μm = 20 ± 6% of cumulative production across controls and treatments).

In contrast, chl *a* dynamics and PP in the microcosms showed different patterns compared to those observed in the mesocosms. Autotrophic standing stocks and production increased in both nutrient-amended treatments (Figs. 4 & 5) to similar maxima, although a decline in biomass and production was observed on Day 6 in the +P treatment. Also, the increase of microorganisms in the >10 μm size fraction was less prominent in the –P microcosm compared to the +P mesocosm (Fig. 4). Cumulative production (the sum of 0–6 d rates) in both nutrient-amended microcosms was similar, increasing ~2× (~50 mg m^{-3}) relative to controls (23 mg m^{-3}) with contributions of the various size-fractions similar to that observed in mesocosms (<2 μm = 43 ± 7% [SD], 2–10 μm = 39 ± 1%, and >10 μm = 17 ± 7% of production across controls and treatments). The most salient difference between microcosms and mesocosms was the diminished absolute magnitude of a production response in the +P treatment observed beginning after ~4 d (Figs. 4 & 5).

3.5. Pigment analyses

Analyses of photosynthetic pigments provided additional insights into the changes in phytoplankton

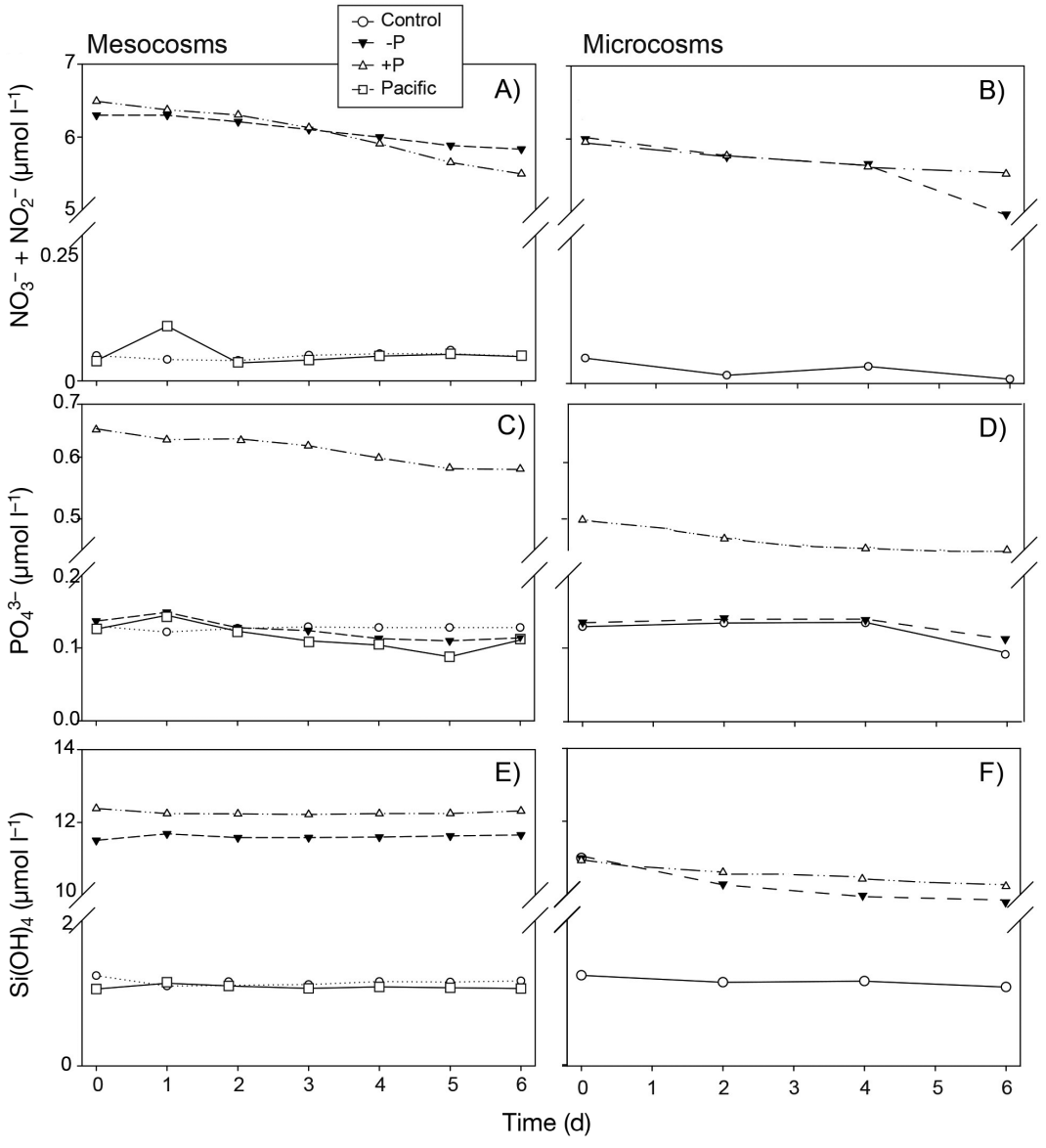

Fig. 3. Dissolved nutrient concentrations in (A,C,E) mesocosms and (B,D,F) microcosms with surrounding near-surface seawater ('Pacific') data (squares) relative to mesocosm data. See Table 2 and Table S8 for raw data. Duplicate samples were not analyzed and hence no error bars are shown

community composition in the 3 mesocosms. Initially, the ratio of 19′-hexanoyloxyfucoxanthin (19′-Hex, marker pigment for Haptophyceae) to monovinyl chl *a* (MChl *a*) was approximately 0.2 in the control and 0.4 in both nutrient-enriched mesocosms (Fig. 6). In addition, the 19′-Hex:MChl *a* ratio was more than twice as high as the ratios of the other 2 marker pigments 19′-butanoyloxyfucoxanthin (19′-But, marker pigment for Pelagophyceae) or fucoxanthin (Fuco, marker pigment for Bacillariophyceae), suggesting a considerable contribution of Haptophyceae at the start of our experiment. Interestingly, the ratio of 19′-Hex:MChl *a* in the control mesocosm steadily increased up to 0.4 towards the end of the experiment, indicating a further increase in Haptophyceae, but decreased to about 50% of its initial contribution (to ~0.2) in the 2 nutrient-enriched mesocosms. Overall, the contribution of either Pelagophyceae or Bacillariophyceae remained relatively minor in the control mesocosm compared to that of Haptophyceae as indicated by 19′-But:MChl *a* and Fuco:MChl *a* ratios of ≤0.1 (Fig. 6). In contrast, ratios of 19′-But:MChl *a* and Fuco:MChl *a* in the 2 nutrient-enriched mesocosms increased during the experiment (Fig. 6). Temporal dynamics of the different pigment to MChl *a* ratios in the surrounding waters were similar to those in the control mesocosms

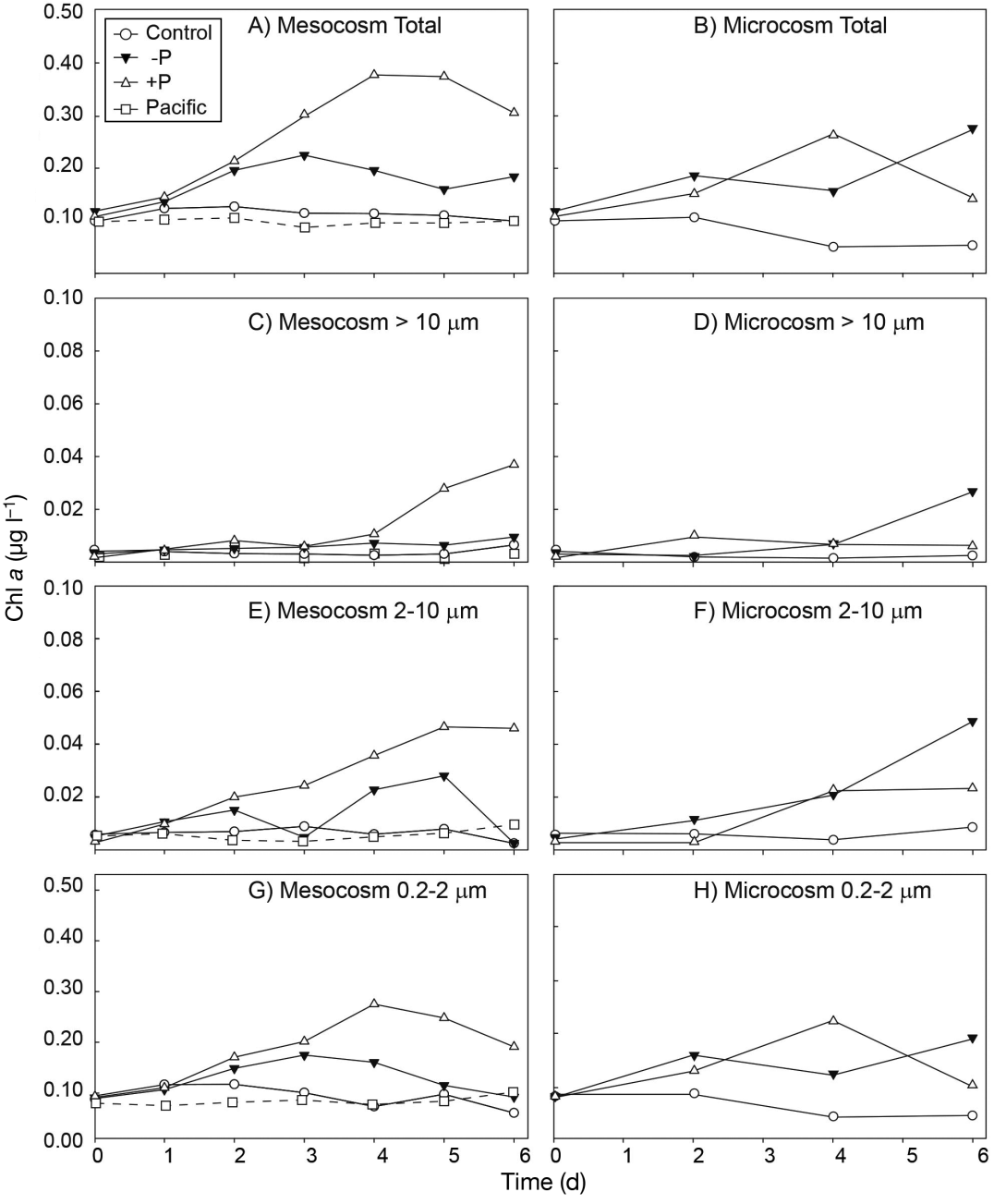

Fig. 4. Temporal development of size-fractionated chlorophyll *a* (chl *a*) concentrations in (A,C,E,G) the 3 mesocosms and (B,D,F,H) the 20 l microcosms. Data from the surrounding Pacific are shown (squares) for comparison. Note the different scales on each panel. Time-zero values for the microcosms are assumed to be equivalent to mesocosm data. Duplicate samples were not collected for these analyses and hence no error bars are shown. All data are provided in Table S5

with a predominance of Haptophyceae throughout the time course of the experiment (data not shown).

3.6. Phytoplankton community structure

Flow cytometric analysis from the 3 mesocosms revealed that PRO was persistently the most abundant of the chlorophyll-containing picoplankton (Fig. 7). Average PRO abundances showed very similar temporal dynamics in the 3 mesocosms, with initial concentrations of ~3.0 × 10^8 cells l^{-1} followed by 3× decreases in the control and +P mesocosm (to ~1.0 × 10^8 cells l^{-1}) and a 6× decline in the −P mesocosm (to ~5 × 10^7 cells l^{-1}; Fig. 7C,D). Concentrations of SYN initially increased in the control mesocosm com-

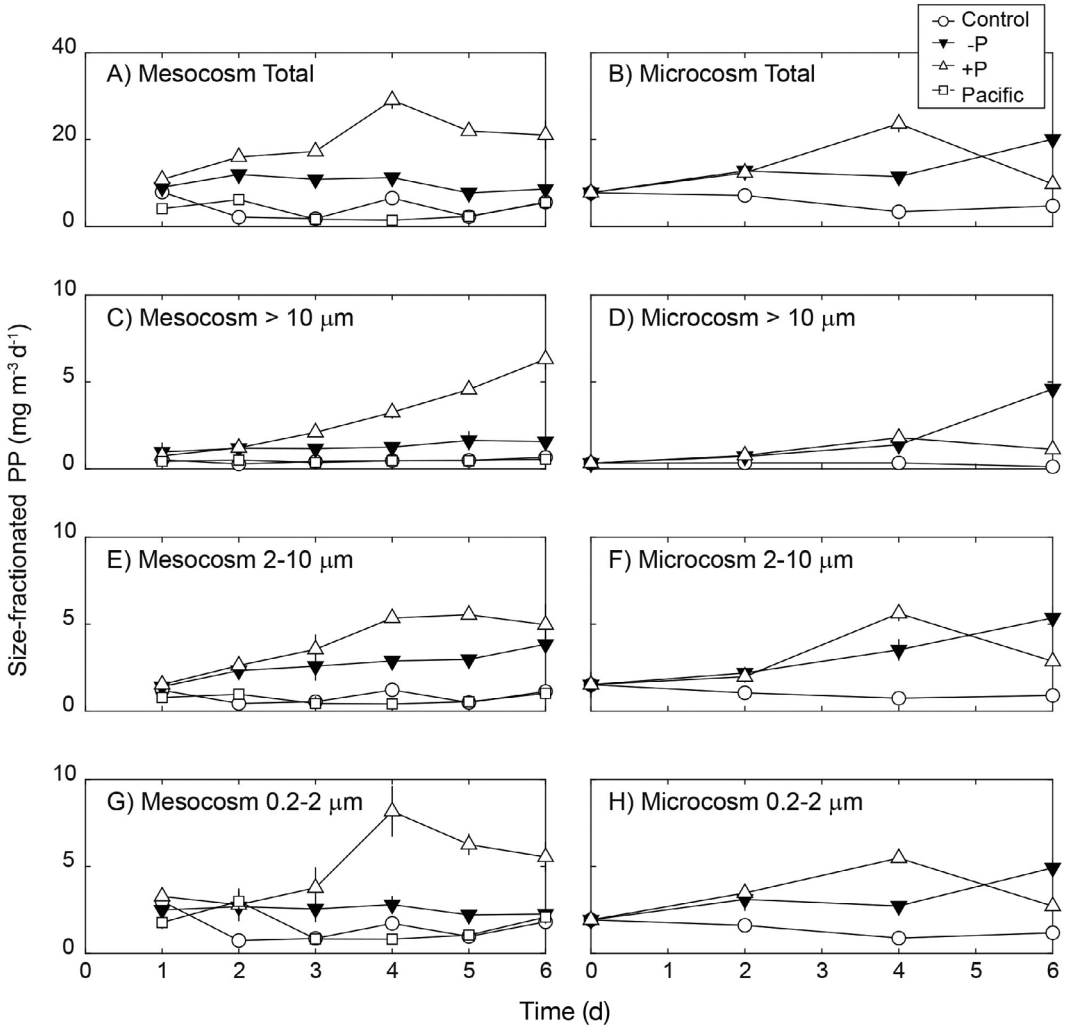

Fig. 5. Daily rates of primary production (PP) of (A,B) total, (C,D) >10 µm, (E,F) 2–10 µm, and (G,H) 0.2–2 µm size fractions (A,C,E,G) in the 3 mesocosms and the surrounding Pacific and (B,D,F,H) in the 20 l microcosms. Error bars represent ±1 SD of the mean rates from sub-samples on each day. Given that mesocosm samples were initiated after dawn, there are no time zero production rates. All data are provided in Table S7

pared to the –P or +P mesocosm, with abundances peaking on Day 3 (~5.0×10^6 cells l^{-1}; Fig. 7E), and progressively decreasing in the latter period of the experiment (to ~3.0×10^6 cells l^{-1}). SYN abundances were highest in the –P mesocosm, with rapid increases occurring between Days 5 and 6, reaching concentrations of nearly 5.0×10^6 cells l^{-1}. Although SYN and PEUK accounted for relatively small fractions of the total photosynthetic picoplankton cell abundances, their relative contributions increased from initially 2 to ~10% in the –P and +P mesocosms. Abundances of HBAC in all 3 treatments were initially ~ 5.0×10^8 cells l^{-1}, increasing by ~3× and 2× in the +P and –P mesocosm, respectively, by the end of the experiment (Fig. 7). The increase in HBAC could also be due to loss of pigmentation of a PRO subpopulation; however, in all mesocosms, the red chlorophyll fluorescence per cell for PRO (Table S9) was either stable (0.02–0.03 in control) or increasing (up to ~0.45 in +P and –P mesocosms).

Qualitative microscopic observations of microphytoplankton were also made in mesocosm-derived samples. Diatoms of the genus *Chaetoceros* sp., *Navicula* sp., and *Skeletonema* sp. were observed to be the dominant microphytoplankton in the +P mesocosm. Microscopic observations from the –P mesocosm indicated the most abundant microphytoplankton species to be *Chaetoceros* spp., *Hemiaulus* spp., and *Leptocylindrus* spp., although at much lower numbers than in the +P treatment.

In microcosms, the decline of PRO was much more pronounced, decreasing to cell concentrations below

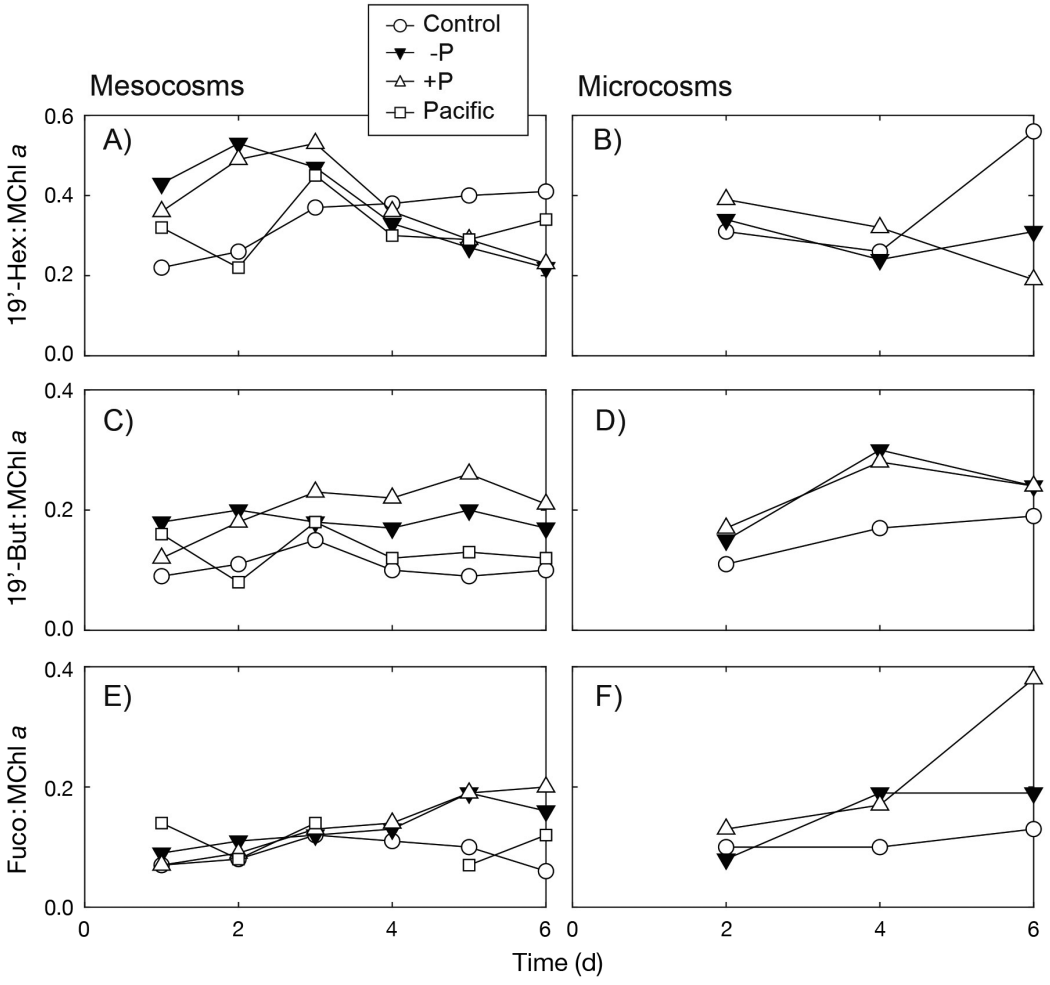

Fig. 6. Temporal dynamics of average pigment to monovinyl chlorophyll *a* (Mchl *a*) ratios in the (A,C,E) mesocosms and the surrounding Pacific and (B,D,F) microcosms are shown for (A,B) 19′-hexanoyloxyfucoxanthin (19′-Hex), (C,D) 19′-butanoyloxyfucoxanthin (19′-But), and (E,F) fucoxanthin (Fuco). Note that due to volume limitations, microcosms were only sampled for pigments on Days 2, 4, and 6, whereas mesocosms were sampled daily; there was insufficient volume for duplicates and hence no error bars. All data are provided in Table S6

0.2×10^6 cells l^{-1} in all treatments by the end of the incubation period (Fig. 7). SYN concentrations increased in the –P microcosm after 4 d, reaching ~3×10^6 cells l^{-1}, similar to abundances observed in the mesocosm treatments. PEUK abundances increased above the controls in both nutrient-amended treatments, reaching the highest values in the –P microcosm (Fig. 7H). In sum, the most dramatic change in cell concentrations across treatments was the overall decrease in PRO in all microcosms and mesocosms after ~2 d, with HBAC increasing in all controls and treatments after ~4 d (Fig. 7).

4. DISCUSSION

Understanding and predicting ecosystem responses to environmental perturbations are fundamental goals in ecology (Moore et al. 2013, Browning et al. 2017), yet the designs of ecosystem perturbation experiments in the open ocean are challenging because physical and biological interactions occur over broad scales of time or space and with ecological complexity that is difficult to examine in small-scale studies (Carpenter 1996, Schindler 1998). Although the mesocosms employed for this study enclosed a relatively large parcel of water, presumably providing a simulated environment 'closer' to the natural environment (Riebesell et al. 2010), caution is still required when extrapolating results across scales (e.g. mesocosm to ecosystem; cf. Schindler 1998), given the lack of experimental replication and the exclusion of trophic assemblages such as diel vertical migrators. Regardless, such large-scale experiments provide insight into potential limitations inherent to smaller

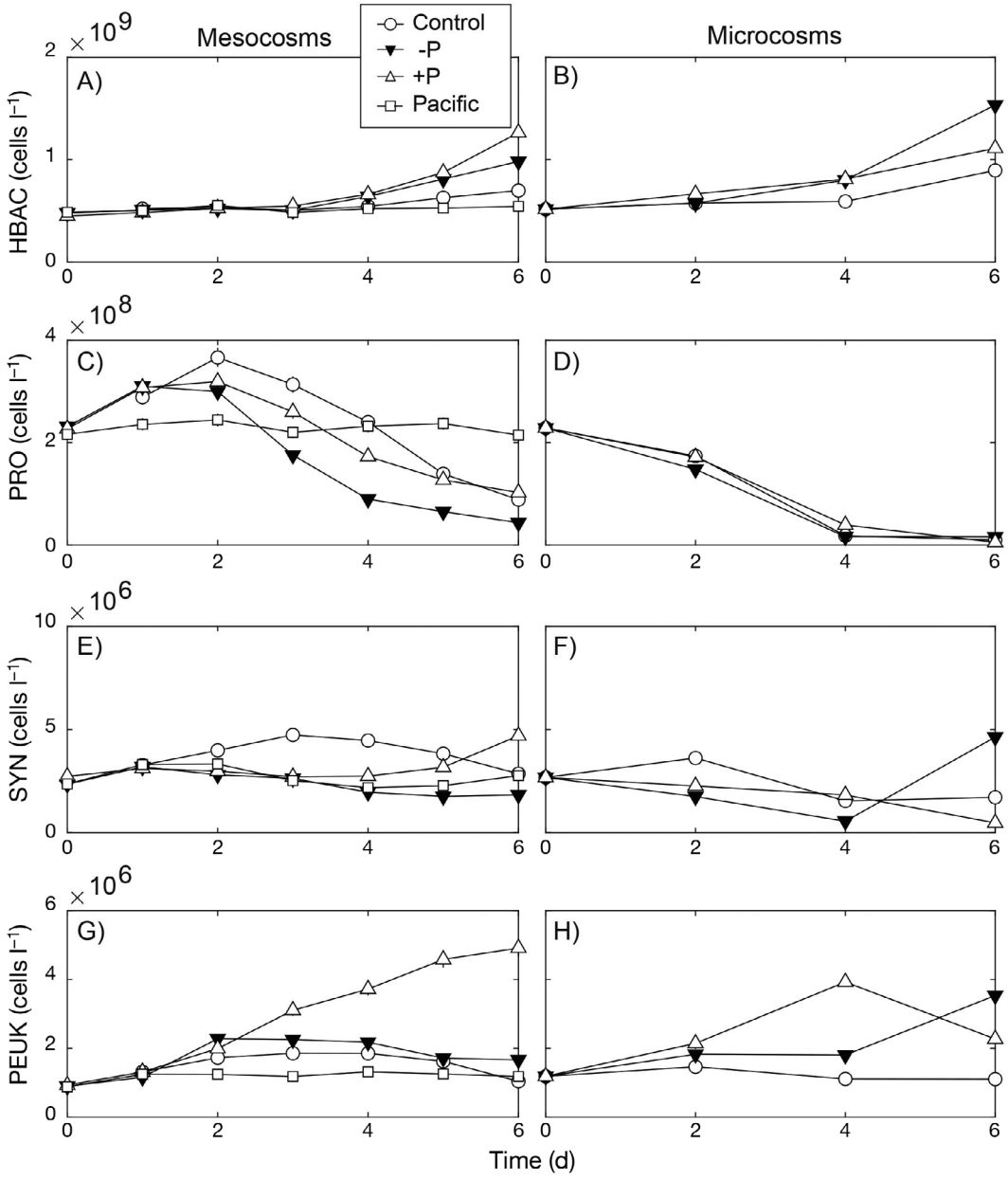

Fig. 7. Daily mesocosm or microcosm (20 l) cell abundances of (A,B) heterotrophic bacteria (HBAC), (C,D) *Prochlorococcus* (PRO), (E,F) *Synechococcus* (SYN), and (G,H) picoeukaryotes (PEUK) in (A,C,E,G) mesocosms and surrounding near-surface seawater ('Pacific') and (B,D,F,H) microcosms. Error bars from duplicate samples are generally smaller than the symbols

microcosm studies. The mesocosm experiments reported in the current study represent a successful first attempt to use the KOSMOS mesocosms in free-drifting mode in an open-ocean environment, where swell, wind, and currents challenge the use of such tools. The study design, while unreplicated, allowed us to investigate the time-dependent responses of upper ocean phytoplankton communities in large-scale mesocosms, and compare the results to those of simultaneous smaller-scale microcosms.

4.1. Response of phytoplankton community to nutrient amendments

Ratios of the dissolved inorganic concentrations of N, P, and Si suggested that phytoplankton biomass and PP in the study area are primarily controlled by the availability and supply of N, with very low N:P and N:Si ratios (mesocosm: 0.3 and 0.04, respectively; microcosm: 0.14 and 0.02, respectively), compared to Redfield ratios (Redfield 1934, Brzezinski

1985). One would therefore predict that the addition of N alone would stimulate phytoplankton biomass and PP in this ecosystem. However, the addition of N along with vitamins and trace metals (–P) did not result in the largest enhancement of phytoplankton biomass and activity in either the microcosm or mesocosm experiment (Figs. 4 & 5). In the mesocosms, the simultaneous addition of N and P plus Si, vitamins, and trace metals resulted in the greatest response by the phytoplankton (reflected by a ~2× increase in total chl *a* and PP relative to –P; Figs. 3A & 4A). Moreover, flow cytometric analyses of fluorescence per cell in photosynthetic picoplankton (Table S9) suggested that the additions of both N and P resulted in changes to cellular physiology. For example, by the end of the mesocosm experiment, per cell fluorescence by both PRO and SYN increased in response to the nutrient additions (PRO: +0.013 cell^{-1} in –P and +0.016 cell^{-1} in +P; SYN: +1.56 cell^{-1} in –P and +1.23 cell^{-1} in the +P; all in units of relative fluorescence per cell) compared to the unamended control (PRO: +0.003 cell^{-1}; SYN: +0.018 cell^{-1}; Table S9). We interpret this as a result of either N and/or Fe additions and subsequent increases in allocation to light-harvesting pigments.

Nutrient enrichments in the mesocosms led to a similar maxima in phytoplankton biomass and production although with differences in the timing (Figs. 4 & 5, Table 2). Whereas the –P and +P mesocosms reached similar maxima in PP and phytoplankton biomass (fluorometric chl *a*), the –P treatment peaked on Day 6 and the +P on Day 4 (Figs. 4 & 5). It is not clear how to explain these 'dips' in biomass and production without additional information on loss terms such as grazing and viral lysis. The production per unit chl *a* was remarkably similar between microcosm treatments (Table S7; ~60–70 g C g^{-1} chl d^{-1}), suggesting that loss of biomass rather than phytoplankton physiology was the cause for the day to day variability.

As expected for the oligotrophic NPSG (Letelier et al. 1993, Liu et al. 1997, Li et al. 2011, Rii et al. 2016), phototrophic assemblages in this study were initially dominated by picoplankton (0.2–2 µm in size), presumably by PRO, contributing approximately 90% to total chl *a* and 60% to ^{14}C-based PP (Figs. 4 & 5). In a persistently low-nutrient environment, high surface area to volume ratios afforded by small cell size likely provides such cells with a competitive advantage over larger phytoplankton, such as diatoms, in the diffusive acquisition of nutrients (Chisholm 1992). However, larger phytoplankton are capable of responding rapidly under conditions where nutrient concentrations increase, often outpacing rates of removal by their predators, leading to the accumulation and subsequent export of organic material. A shift in the phytoplankton community size structure was particularly noted in the +P mesocosm, where increases in concentrations of chl *a* and rates of PP in the >10 µm size fraction (Figs. 4B & 5B) are consistent with growth by larger microphytoplankton cells, most likely diatoms. This interpretation is supported by (1) a notable increase in the ratio of Fuco:MChl *a* (Fig. 6E), a proxy for diatoms (Claustre 1994), and (2) daily qualitative microscopic observations, which revealed increasing abundances in specific diatoms (e.g. *Chaetoceros* sp.) notably in the +P mesocosm. Despite these apparent differences in community structure, the assimilation of Si into particulate matter (PSi) was nearly identical in both nutrient-amended mesocosms over the time course of the experiment (+106 nmol l^{-1} in –P and +107 nmol l^{-1} in +P) and the Fuco:MChl *a* ratio in the –P mesocosm increased to similar values compared to those in the +P mesocosm (~0.2; Fig. 6E). Similar increases in Fuco:MChl *a* ratio were observed in microcosms (Fig. 6F). We suspect that diatoms or silicoflagellates <10 µm responded in the nutrient-amended mesocosm and to a lesser extent in the microcosms, assimilating Si, which at the same time would explain the increased Fuco:MChl *a* ratio as well as chl *a* and PP in the 2–10 µm fraction observed in this mesocosm (Figs. 4C & 5E,F). However, in both mesocosm and microcosm treatments, the decline of PRO populations was apparent, albeit less dramatically so in mesocosms (Fig. 7).

Previous inorganic nutrient addition experiments, conducted in oligotrophic ocean ecosystems and relying on microcosm-sized incubations, have found comparable time scales in the responses of phytoplankton biomass and production (Zohary et al. 2005, McAndrew et al. 2007, Mahaffey et al. 2012, Rii et al. 2018). Limitations in our experimental design, specifically the constraint of having only 3 mesocosms, preclude determination of limiting nutrients, including possible co-limitation by N and P or N and trace elements (Saito et al. 2008). However, it is clear that N is not the sole determinant of enhanced PP in this study. A factorial design would be needed to tease apart which elements may be limiting *in situ* growth. The constancy in daily chl *a* and PP measurements in the control mesocosm provides confidence that the observed phytoplankton response in the nutrient-amended mesocosms was not an artifact of containment inside the mesocosm bag. Also, the temporal dynamics in the control mesocosm closely followed

those in the surrounding Pacific Ocean, which further suggests that possible 'bag effects' were minimized (Table S7). Pulses of inorganic nutrients to the surface ocean via mixing, eddies, or in experimental manipulations have been shown to select for large-sized microphytoplankton (Benitez-Nelson et al. 2007, Dore et al. 2008, Karl & Letelier 2008, Mahaffey et al. 2012), thereby shifting the metabolic state from net heterotrophy or a closely balanced system to net autotrophy (McAndrew et al. 2007). Thus, the shift in the phytoplankton community size structure from small, <2 µm phytoplankton (PRO, SYN) to large >2 µm phytoplankton (PEUKs and diatoms) in the present study is not surprising.

4.2. Comparison of microcosm and mesocosm dynamics

Replication of large-scale experiments is undoubtedly desirable, but costs and logistics associated with these experimental approaches may be prohibitive (Boyd et al. 2018). The present experiment was first and foremost intended as an engineering test, hence the limited number of mesocosms (n = 3). Similar replication issues have been confronted by studies conducting mesoscale iron fertilization experiments (Hale & Rivkin 2007) and are to be expected in large-scale experiments. Nevertheless, we are confident that the results obtained in this study constitute a valuable first step towards scaling plankton manipulation experiments in the open ocean. The lack of replication is a persistent logistical hurdle often observed in large-volume experiments such as whole lake manipulations (Carpenter et al. 1998) or open ocean iron fertilization studies (de Baar et al. 2005).

In general, the magnitude of the phytoplankton responses to nutrient perturbations in the mesocosms and microcosms were comparable; however, there were key differences in the timing of the responses and the plankton community structure, with diatom growth more apparent in mesocosms. These differences cannot be easily explained without additional information such as grazing pressure. Furthermore, we are fully aware that the duration of the present experiment might have been too short to investigate the entire plankton succession, and a continued buildup of larger-sized phytoplankton over time could have been expected with such a vast pool of unutilized nutrients (~5 µmol N l^{-1}). Yet, community composition in mesocosms was more consistent with natural populations; the comparison between the mesocosm and microcosm results reveal slower PRO decline over the full incubation period and even growth in the initial 2 d in mesocosms, suggesting variable trophic interactions in larger-volume incubations. Given the relatively stable fluorescence per cell for PRO (Table S9) and the rise of HBAC in both mesocosms and microcosms (Fig. 7), we interpret this as cell death potentially fueling bacterial populations. The loss of PRO has been documented in other mesocosm studies; a prominent decline in PRO was observed in stationary mesocosm studies in Gando Bay, Gran Canaria (Spain), where PRO was present (~10^4–10^5 cells ml^{-1}) during the first few days of the experiment, but began to rapidly decline to undetectable levels by 10 d in treatments and controls alike (Taucher et al. 2018). This suggests that even large-volume containments will impede net growth of PRO for reasons not yet understood. In contrast, SYN, and PEUK cell concentrations were similar in microcosms and mesocosms. PRO is sensitive to ultraviolet radiation levels (Llabrés & Agustí 2006) and is reliant on specific interactions with co-occurring HBAC (Roth-Rosenberg et al. 2020); perturbation of the incoming light-spectrum or diversity of the HBAC diversity (although not measured) may be responsible for the low survival of PRO in incubations.

Mesocosm manipulation experiments such as performed here offer the potential for highly controlled mechanistic insights into the relationship between nutrient injections and the physiological and ecological responses of plankton communities and their biogeochemical impacts. Our results highlight the successful (and, to our knowledge, first) deployment of free-drifting mesocosms in the open ocean and illustrate significant changes in community composition and production as compared to the more traditional microcosms. The observed differences may be the result of variable predator–prey interactions in microcosms relative to mesocosms or due to *in situ* versus simulated environmental conditions. While we do not have the data on hand to understand these differences fully, we believe our results reiterate the need to carefully consider the scale of incubations in interpreting the physiological response of microbial communities to nutrient perturbations and their impacts on ecological interactions and elemental fluxes.

Acknowledgements. We thank the National Science Foundation (C-MORE; award EF-0424599), the Gordon and Betty Moore Foundation (#3794 to D.M.K.), and the Simons Foundation (Award #329104) for their support of this study. This research could not have been accomplished without the support and expertise of the captain and crew of the RV *Ka'imikai-O-Kanaloa* and the diving operations conducted by the UH and GEOMAR diving personnel J. Büdenbender,

J. Czerny, M. Fisher, D. Pence, and J. Mowatt. We are extremely grateful to B. Watkins, J. Czerny, D. Hoffmann, and B. Updyke for their enormous efforts in assembling the 3 mesocosms prior to the campaign. We also acknowledge the expertise of J. Büdenbender, J. Czerny, M. Fischer, and B. Watkins during deployment and daily sampling; E. Grabowski provided video recording and help with particulate matter analyses; and R. Bidigare provided HPLC analyses. Many thanks to the remaining cruise participants T. Clemente, K. Doggett, C. Schvarcz, S. Tozzi, and K. Watkins-Brandt for their support during the campaign.

LITERATURE CITED

Benitez-Nelson CR, Bidigare RR, Dickey TD, Landry MR and others (2007) Mesoscale eddies drive increased silica export in the subtropical Pacific Ocean. Science 316: 1017–1021

Bidigare RR, Van Heukelem L, Trees CC (2005) Analysis of algal pigments by high-performance liquid chromatography. In: Anderson RA (ed) Algal culturing techniques. Academic Press, New York, NY, p 327–345

Boyd PW (2008) Ranking geo-engineering schemes. Nat Geosci 1:722–724

Boyd PW, Collins S, Dupont S, Fabricius K and others (2018) Experimental strategies to assess the biological ramifications of multiple drivers of global ocean change — a review. Glob Change Biol 24:2239–2261

Browning TJ, Achterberg EP, Rapp I, Engel A, Bertrand EM, Tagliabue A, Moore CM (2017) Nutrient co-limitation at the boundary of an oceanic gyre. Nature 551:242–246

Brzezinski MA (1985) The Si:C:N ratio of marine diatoms: interspecific variability and the effect of some environmental variables. J Phycol 21:347–357

Carpenter SR (1996) Microcosm experiments have limited relevance for community and ecosystem ecology. Ecology 77:677–680

Carpenter SR, Cole JJ, Essington TE, Hodgson JR, Houser JN, Kitchell JF, Pace ML (1998) Evaluating alternative explanations in ecosystem experiments. Ecosystems 1:335–344

Chisholm SW (1992) Phytoplankton size. In: Falkowski PG, Woodhead AD (eds) Primary productivity and biogeochemical cycles in the sea. Environmental science research, Book 43. Springer, Boston, MA, p 213–237

Claustre H (1994) The trophic status of various oceanic provinces as revealed by phytoplankton pigment signatures. Limnol Oceanogr 39:1206–1210

Crawfurd KJ, Alvarez-Fernandez S, Mojica KD, Riebesell U, Brussaard CP (2017) Alterations in microbial community composition with increasing fCO_2: a mesocosm study in the eastern Baltic Sea. Biogeosciences 14: 3831–3849

de Baar HJW, Boyd PW, Coale KH, Landry MR and others (2005) Synthesis of iron fertilization experiments: from the Iron Age in the Age of Enlightenment. J Geophys Res Oceans 110:C09S16

DeMaster DJ (1981) The supply and accumulation of silica in the marine environment. Geochim Cosmochim Acta 45:1715–1732

Dore JE, Letelier RM, Church MJ, Lukas R, Karl DM (2008) Summer phytoplankton blooms in the oligotrophic North Pacific Subtropical Gyre: historical perspective and recent observations. Prog Oceanogr 76:2–38

Edler L, Elbrächter M (2010) The Utermöhl method for quantitative phytoplankton analysis. In: Karlson B, Cusack C, Bresnan E (eds) Microscopic and molecular methods for quantitative phytoplankton analysis, Book 110. UNESCO, Paris, p 13–21

Endres S, Galgani L, Riebesell U, Schulz KG, Engel A (2014) Stimulated bacterial growth under elevated pCO_2: results from an off-shore mesocosm study. PLOS ONE 9: e99228

Estrada M, Berdalet E, Vila M, Marrasé C (2003) Effects of pulsed nutrient enrichment on enclosed phytoplankton: ecophysiological and successional responses. Aquat Microb Ecol 32:61–71

Fong AA, Karl DM, Lukas R, Letelier RM, Zehr JP, Church MJ (2008) Nitrogen fixation in an anticyclonic eddy in the oligotrophic North Pacific Ocean. ISME J 2:663–676

Gamble JC, Davies JM (1982) Application of enclosures to the study of marine pelagic systems. In: Grice GD, Reeve MR (eds) Marine mesocosms. Springer, New York, NY, p 25–48

Grabowski E, Letelier RM, Laws EA, Karl DM (2019) Coupling carbon and energy fluxes in the North Pacific Subtropical Gyre. Nat Commun 10:1895

Hale MS, Rivkin RB (2007) Interpreting the results of oceanic mesoscale enrichment experiments: caveats and lessons from limnology and coastal ecology. Limnol Oceanogr 52:912–916

Hecky R, Kilham P (1988) Nutrient limitation of phytoplankton in freshwater and marine environments: a review of recent evidence on the effects of enrichment 1. Limnol Oceanogr 33:796–822

Holm-Hansen O, Lorenzen CJ, Holmes RW, Strickland JD (1965) Fluorometric determination of chlorophyll. ICES J Mar Sci 30:3–15

Karl DM, Letelier RM (2008) Nitrogen fixation-enhanced carbon sequestration in low nitrate, low chlorophyll seascapes. Mar Ecol Prog Ser 364:257–268

Karl D, Bidigare R, Letelier R (2001) Long-term changes in plankton community structure and productivity in the North Pacific Subtropical Gyre: the domain shift hypothesis. Deep Sea Res II 48:1449–1470

Letelier RM, Bidigare RR, Hebel DV, Ondrusek M, Winn C, Karl DM (1993) Temporal variability of phytoplankton community structure based on pigment analysis. Limnol Oceanogr 38:1420–1437

Letelier R, Dore J, Winn C, Karl D (1996) Seasonal and interannual variations in photosynthetic carbon assimilation at Station ALOHA. Deep Sea Res II 43:467–490

Letelier RM, Karl DM, Abbott MR, Bidigare RR (2004) Light driven seasonal patterns of chlorophyll and nitrate in the lower euphotic zone of the North Pacific Subtropical Gyre. Limnol Oceanogr 49:508–519

Letelier RM, Björkman KM, Church MJ, Hamilton DS and others (2019) Climate-driven oscillation of phosphorus and iron limitation in the North Pacific Subtropical Gyre. Proc Natl Acad Sci USA 116:12720–12728

Li B, Karl DM, Letelier RM, Church MJ (2011) Size-dependent photosynthetic variability in the North Pacific Subtropical Gyre. Mar Ecol Prog Ser 440:27–40

Liu H, Nolla HA, Campbell L (1997) *Prochlorococcus* growth rate and contribution to primary production in the equatorial and subtropical North Pacific Ocean. Aquat Microb Ecol 12:39–47

Llabrés M, Agustí S (2006) Picophytoplankton cell death induced by UV radiation: evidence for oceanic Atlantic communities. Limnol Oceanogr 51:21–29

Lovelock JE, Rapley CG (2007) Ocean pipes could help the Earth to cure itself. Nature 449:403

Mahaffey C, Björkman KM, Karl DM (2012) Phytoplankton response to deep seawater nutrient addition in the North Pacific Subtropical Gyre. Mar Ecol Prog Ser 460:13–34

McAndrew PM, Björkman KM, Church MJ, Morris PJ, Jachowski N, Williams PJ, Karl DM (2007) Metabolic response of oligotrophic plankton communities to deep water nutrient enrichment. Mar Ecol Prog Ser 332:63–75

Moore CM, Mills MM, Arrigo KR, Berman-Frank I and others (2013) Processes and patterns of oceanic nutrient limitation. Nat Geosci 6:701–710

Redfield AC (1934) On the proportions of organic derivatives in sea water and their relation to the composition of plankton. James Johnstone Memorial Volume. University Press of Liverpool, p 176–192

Redfield AC (1958) The biological control of chemical factors in the environment. Am Sci 46:230A–221

Riebesell U, Fabry V, Hansson L, Gattuso J (2010) Guide to best practices in ocean acidification research and data reporting. Report of international research workshop on best practices for ocean acidification research (19–21 November 2008 in Kiel, Germany). European Commission, Brussels

Riebesell U, Czerny J, von Bröckel K, Boxhammer T and others (2013) Technical Note: a mobile sea-going mesocosm system — new opportunities for ocean change research. Biogeosciences 10:1835–1847

Rii YM, Brown SL, Nencioli F, Kuwahara V, Dickey T, Karl DM, Bidigare RR (2008) The transient oasis: nutrient–phytoplankton dynamics and particle export in Hawaiian lee cyclones. Deep Sea Res II 55:1275–1290

Rii YM, Karl DM, Church MJ (2016) Temporal and vertical variability in picophytoplankton primary productivity in the North Pacific Subtropical Gyre. Mar Ecol Prog Ser 562:1–18

Rii YM, Bidigare RR, Church MJ (2018) Differential responses of eukaryotic phytoplankton to nitrogenous nutrients in the North Pacific Subtropical Gyre. Front Mar Sci 5:92

Roth-Rosenberg D, Aharonovich D, Luzzatto-Knaan T, Vogts A and others (2020) *Prochlorococcus* cells rely on microbial interactions rather than on chlorotic resting stages to survive long-term nutrient starvation. mBio 11: e01846-20

Saito MA, Goepfert TJ, Ritt JT (2008) Some thoughts on the concept of colimitation: three definitions and the importance of bioavailability. Limnol Oceanogr 53:276–290

Schindler DW (1998) Whole-ecosystem experiments: replication versus realism: the need for ecosystem-scale experiments. Ecosystems 1:323–334

Smith S, Mackenzie F (1991) Comments on the role of oceanic biota as a sink for anthropogenic CO_2 emissions. Global Biogeochem Cycles 5:189–190

Steemann Nielsen E (1952) The use of radio-active carbon (C^{14}) for measuring organic production in the sea. ICES J Mar Sci 18:117–140

Sunda WG (2012) Feedback interactions between trace metal nutrients and phytoplankton in the ocean. Front Microbiol 3:204

Takahashi T, Feely RA, Weiss RF, Wanninkhof RH, Chipman DW, Sutherland SC, Takahashi TT (1997) Global air–sea flux of CO_2: an estimate based on measurements of sea–air pCO_2 difference. Proc Natl Acad Sci USA 94:8292–8299

Taucher J, Arístegui J, Bach LT, Guan W and others (2018) Response of subtropical phytoplankton communities to ocean acidification under oligotrophic conditions and during nutrient fertilization. Front Mar Sci 5:330

Vaughan NE, Lenton TM (2011) A review of climate geoengineering proposals. Clim Change 109:745–790

White AE, Spitz YH, Letelier RM (2007) What factors are driving summer phytoplankton blooms in the North Pacific Subtropical Gyre? J Geophys Res Oceans 112: C12006

Worden AZ, Not F (2008) Ecology and diversity of picoeukaryotes. In: Kirchman DL (ed) Microbial ecology of the oceans, 2nd edn. John Wiley & Sons, , Hoboken, NJ, p 159–206

Zohary T, Herut B, Krom MD, Mantoura RFC and others (2005) P-limited bacteria but N and P co-limited phytoplankton in the Eastern Mediterranean — a microcosm experiment. Deep Sea Res II 52:3011–3023

Editorial responsibility: Ilana Berman-Frank, Haifa, Israel
Reviewed by: 3 anonymous referees

Submitted: September 28, 2020
Accepted: July 28, 2021
Proofs received from author(s): October 8, 2021